Monthly Notices of the ROYAL ASTRONOMICAL SOCIETY

MNRAS **453,** 2050–2057 (2015) doi:10.1093/mnras/stv1762

Cold galaxies

Michael Rowan-Robinson★ and David L. Clements

Astrophysics Group, Blackett Laboratory, Imperial College London, Prince Consort Road, London SW7 2AZ, UK

Accepted 2015 July 29. Received 2015 July 29; in original form 2015 May 4

ABSTRACT

We use 350 μm angular diameter estimates from *Planck* to test the idea that some galaxies contain exceptionally cold (10–13 K) dust, since colder dust implies a lower surface brightness radiation field illuminating the dust, and hence a greater physical extent for a given luminosity. The galaxies identified from their spectral energy distributions as containing cold dust do indeed show the expected larger 350 μm diameters. For a few cold dust galaxies where *Herschel* data are available, we are able to use submillimetre maps or surface brightness profiles to locate the cold dust, which as expected generally lies outside the optical galaxy.

Key words: stars: formation – galaxies: evolution – galaxies: starburst – cosmology: observations – infrared: galaxies.

1 INTRODUCTION

One of the surprising results from submillimetre (sub-mm)surveys with *Herschel* and *Planck* has been the discovery that some local ($z < 0.1$) quiescent galaxies show spectral energy distributions (SEDs) characteristic of cold ($T = 10$–13 K) dust (Planck Collaboration XVI 2011; Rowan-Robinson et al. 2010, 2014; Wang et al. 2014). Two examples are illustrated in Fig. 1.

Cold dust in sub-mm galaxies has also been investigated by Galametz et al. (2012), Smith et al. (2012) and Symeonidis et al. (2013) using SED fitting, by Bourne et al. (2013) using CO and by Ibar et al. (2013) using C II. Bendo et al. (2015) have used surface brightness ratios at 250, 350 and 500 μm to explore the relative contribution of newly formed and old stars to dust heating.

To test the idea that exceptionally cold dust is present in some galaxies we compare *Planck* 350 μm diameters with diameters estimated from radiative transfer models for the far-infrared and sub-mm emission. We also look at sub-mm maps for selected galaxies derived from *Herschel* data. Broadly speaking, we expect to find that galaxies with colder dust will be more extended spatially at sub-mm wavelengths than normal galaxies of the same luminosity.

The structure of this paper is as follows: in Section 2 we estimate the sub-mm diameters for galaxies with cool and cold dust and compare these with predictions for normal cirrus galaxies, in Section 3 we compare these predictions with the 350 μm diameters observed by *Planck* and in Section 4 we discuss the few cases where we have *Herschel* maps for cold dust galaxies. Section 5 gives our discussion and conclusions.

2 PREDICTED SUB-MM DIAMETERS

The temperature of optically thin interstellar dust ('cirrus') is determined by the intensity of the interstellar radiation field, which can be characterized by the ratio of the intensity of the radiation field to the local solar neighbourhood interstellar radiation field, ψ (Rowan-Robinson 1992, hereafter RR92). The standard cirrus template of Rowan-Robinson et al. (2005, 2008, 2013) corresponds to $\psi = 5$, and this is the value used by RR92 to fit the central regions of our Galaxy. $\psi = 1$ corresponds to the interstellar radiation field in the vicinity of the Sun ('cool' dust). Rowan-Robinson et al. (2010, 2014) found that some *Herschel* galaxies need a much lower intensity radiation field than this, with $\psi = 0.1$ ('cold' dust). A similar result was found for some *Planck* galaxies by Planck Collaboration XVI (2011). The corresponding grain temperatures in the dust model of RR92 are given in table 1 of Rowan-Robinson et al. (2010). For the three values of $\psi = 5, 1, 0.1$, the ranges of dust grain temperatures for the different grain types are 20–24 K, 14.5–19.7 K and 9.8–13.4 K, respectively. Full details of the templates used are given via a readme page.[1]

One of the ways to test these ideas is to measure the sub-mm diameter. Since $\psi = 1$ corresponds to the intensity in the solar neighbourhood, we can estimate the sub-mm diameter of galaxies by

$$\theta \sim 2R_0\psi^{-0.5}(zc\tau_0)^{-1}(L_{\rm ir}/L_{\rm MW})^{-0.5}, \quad (1)$$

where $R_0 = 8.5$ kpc, the distance of the Sun from the Galactic Centre, and $L_{\rm MW} = 2.4 \times 10^{10}\,{\rm L}_\odot$. The definition of ψ in the solar neighbourhood is in terms of a mean surface brightness and so we can expect that θ defined by this equation is essentially a full width to half-power when observing external galaxies.

★ E-mail: mrr@imperial.ac.uk

[1] http://astro.ic.ac.uk/public/mrr/swirephotzcat/templates/readme

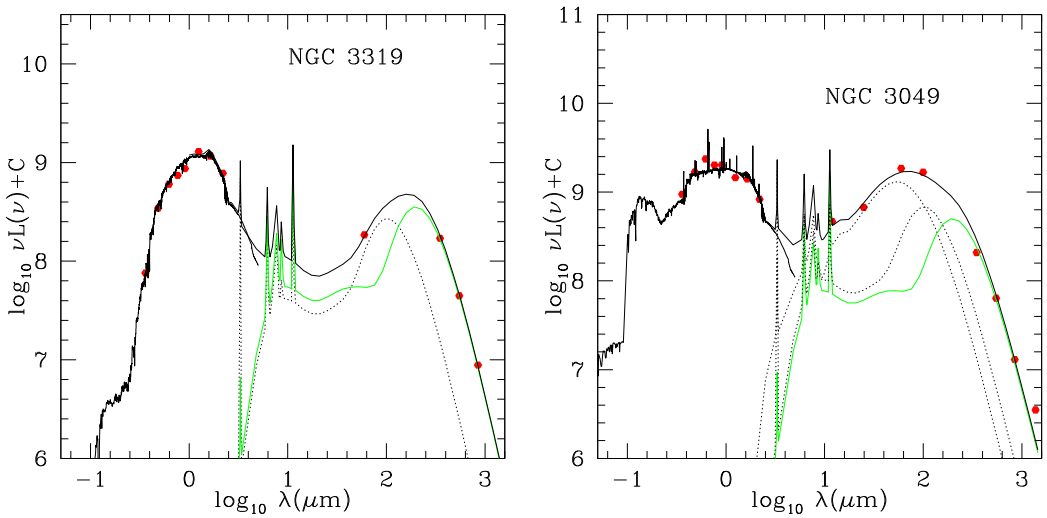

Figure 1. SEDs of NGC 3319 and NGC 3049, showing need for cold dust component (green).

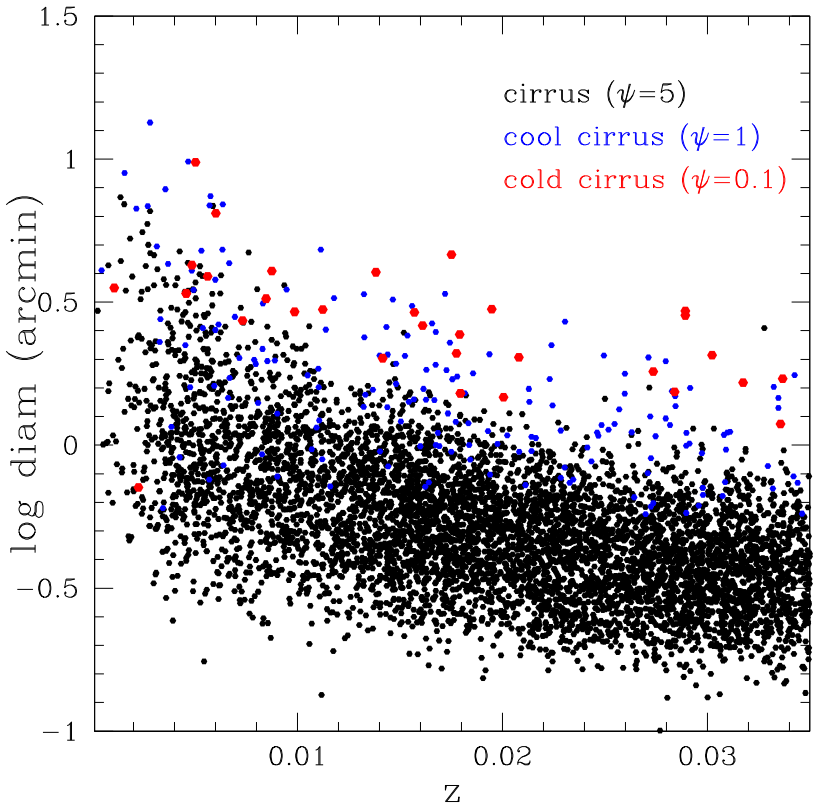

Figure 2. Predicted sub-mm diameter versus redshift for cirrus ($\psi = 5$) galaxies (black), cool galaxies ($\psi = 1$, blue) and cold galaxies ($\psi = 0.1$, red).

Fig. 2 shows a plot of the predicted angular size, θ, versus redshift for galaxies in the RIFSCz *IRAS* galaxy redshift catalogue (Wang et al. 2014) whose far-infrared and sub-mm emission is best fitted by standard cirrus or cool cirrus, for the sample of Planck galaxies identified as requiring cold dust by Planck Collaboration XVI (2011), and for the RIFSCz galaxies identified as needing cold dust templates by Wang et al. (2014). The prediction is that galaxies with significant cool or cold dust components should have larger sub-mm diameters than their normal cirrus counterparts. Table 1 summarizes the properties of the cold dust galaxies from these latter two papers.

3 MEASURED *PLANCK* 350 μM DIAMETERS

We have focused on those galaxies for which the predicted sub-mm diameter is greater than 3 arcmin and compared these with the PCCS sub-mm diameters (FWHM) observed by *Planck* at 350 μm. We use the Gaussian half-power width measured along the major axis. Table 2 summarizes the properties of galaxies from the *IRAS* RIFSCz catalogue with predicted sub-mm diameter greater than 3 arcmin, spectroscopic redshifts, at least eight optical photometric bands, χ^2 for the infrared template fit <5 and SEDs dominated either by a cirrus or cool dust template. Fig. 3L shows a comparison

Table 1. Galaxies requiring cold dust components.

IRAS name	z	L_{opt}	$\log_{10}\theta_{pred}$	θ_{Planck}	$\log_{10}\theta_{opt}$	ncirr	Name
(a) *Planck* selected							
F10361+4155	0.002 228	7.50	0.63	6.57	0.79	1	NGC 3319
F14302+1006	0.004 57	9.48	0.53	5.61	0.65	1	NGC 5669
F09521+0930	0.004 85	9.73	0.62	5.24	0.40	1	NGC 3049
F10290+6517	0.005 62	9.78	0.59	11.53	0.36	3	NGC 3259
F14004+5603	0.006 01	10.28	0.81	5.3	0.52	1	NGC 5443
F15122+5841	0.008 47	9.98	0.51	7.7	−0.21	3	MrK0847
F15248+4044	0.008 74	10.20	0.62	6.1	0.65	1	UGC09858
F14366+0534	0.005 02	10.48	0.99	10.39	0.65	3	NGC 5701
F13405+6101	0.007 32	9.70	0.43	6.71	0.23	1	UGC08684
F08233+2303	0.017 94	9.97	−0.03				KUG0823+230B
F15243+5237	0.019 48	10.63	0.36				UGC09853
F15495+5545	0.039 74	10.90	−0.54				SBS1549+557
F04257-4913	0.058 28	11.85	−0.10				ESO202-IG021
(b) RIFSCz selected							
F12234+3348	0.001 060	8.25	0.550		1.12		NGC 4395
F23461+0353	0.009 860	10.02	0.466		0.40		NGC 7757
F11555+2809	0.011 230	10.15	0.475		0.26		NGC 4004
F02533+0029	0.013 820	10.59	0.604		0.15		UGC02403
F12208+0744	0.014 160	10.01	0.304		0.36		NGC 4334
F15097+2129	0.015 700	10.42	0.464		0.18		UGC09763
F00342+2342	0.016 110	10.35	0.418		0.43		NGC 169 (Arp282)
F08070+3406	0.017 520	10.92	0.666		0.35		NGC 2532
F14280+2158	0.017 750	10.24	0.321		0.19		UGC09316
F07581+3259	0.017 910	10.38	0.387		−0.24		CGCG178-018
F08277+2046	0.020 050	10.04	0.168		0.05		UGC04446
F09388+1138	0.020 810	10.35	0.307		0.36		UGC05173
F13090+4658	0.027 370	10.49	0.258		−0.23		UGC08269
F14236+0528	0.028 400	10.38	0.187		−0.41		UGC09244
F23254+0830	0.028 920	10.96	0.469		0.06		NGC 7674
F08199+0427	0.028 930	10.93	0.454		−0.31		CGCG032-009
F11078+0505	0.030 230	10.69	0.315		−0.24		UGC06212
F15426+4115	0.031 750	10.54	0.218		−0.05		NGC 5992
F16269+4013	0.033 570	10.30	0.074		−0.38		KUG1626+402
F14547+2449	0.033 670	10.62	0.233		−0.18		UGC09618

of the observed *Planck* diameters with the optical diameters, taken from the 3rd Reference Catalogue of Galaxies, for the galaxies of Tables 1 and 2. The quoted *Planck* beam at 350 μm is 4.3 arcmin (FWHM); so we deconvolve both the telescope beam and source profile can be approximated as Gaussians. Fig. 3R shows the observed diameters using $\theta_{deconv} = (\theta^2 - 4.3^2)^{-1/2}$, assuming that both the telescope beam and the source profile can be approximated as Gaussians (adaquate for our purposes). Values of $\theta_{deconv} < 4$ arcmin will be subject to considerable uncertainty. Fig. 3R shows a comparison of the deconvolved *Planck* diameters with the predicted values from equation (1). All three types are consistent with a simple linear relation, apart from a cluster of galaxies with anomalously high *Planck* diameters, which we suggest are affected by Galactic cirrus (most have high cirrus flags in the *Planck* PCCS, e.g. NGC 1024, 3573, 4650 and IC 4831 and 5078). We have fitted straight lines through the origin to these three distributions and find slopes 1.38 ± 0.13 for 40 normal cirrus galaxies, 1.16 ± 0.09 for 64 cool galaxies (excluding eight probable cirrus sources) and 1.32 ± 0.21 for eight cold galaxies. Thus, all three populations show statistically significant correlations between the observed and predicted diameters, the slopes are consistent with being the same in each case and are also not inconsistent with the true slope being unity.

There are also two outliers with rather large predicted diameters, NGC 6744 and M104. Figs 4L and 5 show the SEDs for these two outliers. For NGC 6744, once the *IRAS* fluxes from the *IRAS* Large Galaxy Catalogue (Rice et al. 1988) have been used, the SED is in fact dominated by a standard cirrus template, so it should move to the left in Fig. 3R. For M104, Bendo et al. (2006) have suggested that the active galactic nucleus at the centre of the galaxy contributes to the sub-mm emission. Fig. 4R shows *Herschel* 250 μm contours superposed on an *i*-band image for M104 ('The Sombrero'). The 250 μm emission arises from a ring of dust outside the main distribution of starlight. The predicted value of θ may also be an overestimate because in this edge-on system, the starlight illuminating the dust ring has been significantly attenuated by dust in the disc of the galaxy, so again this object should move to the left in Fig. 3R.

4 RESULTS FROM MAPS OF SELECTED SOURCES

Mapping data in the sub-mm from the SPIRE instrument (Griffin et al. 2010) on the *Herschel Space Observatory* (Pilbratt et al. 2010) is available for a few of the galaxies identified here as containing cold dust. This allows us to compare the location of the dust responsible for the sub-mm emission with the location of the starlight.

Two of the sources (NGC 5701 and NGC 5669) were observed as part of the *Herschel* Reference Survey (Boselli et al. 2010) and a third (NGC 3049) was observed by the KINGFISH programme (Kennicutt et al. 2010). The SPIRE images were obtained from the *Herschel* or HerMES data archives.

Table 2. Comparison samples of large galaxies requiring cool dust or normal cirrus components.

IRAS name Cool dust galaxies	z	$L_{\rm opt}$	$\log_{10}\theta_{\rm pred}$	θ_{Planck}	$\log_{10}\theta_{\rm opt}$	ncirr	Name
F00380−1408	0.005 460	11.17	0.798	7.30	0.70	1	NGC 0210
F00446−2101	0.000 520	9.29	0.879	13.11	1.34	2	NGC 0247
F01191+0459	0.007 580	11.24	0.690	6.43	0.73	1	NGC 0488
F01443+3519	0.015 590	11.46	0.487	13.7	0.51	4	NGC 0669
F02364+1037	0.011 780	11.27	0.514	18.46	0.62	7	NGC 1024
F02403+3707	0.001 730	9.60	0.512	6.85	0.51	1	NGC 1058
F02415−2912	0.004 840	10.69	0.610	7.81	0.53	1	NGC 1079
F03116−0300	0.005 710	10.85	0.618	8.44	0.73	1	NGC 1253
F03151−3245	0.015 140	11.44	0.490	4.90	0.36	1	NGC 1288
F03174−1935	0.005 260	11.07	0.764	6.77	0.80	1	NGC 1300
F03222−2143	0.005 310	10.91	0.680	5.56	0.68	2	NGC 1325
F03291−3348	0.006 350	11.39	0.842	5.80	0.72	1	NGC 1350
F03309−1349	0.006 660	11.02	0.637	11.27	0.45	2	NGC 1357
F03367−2629	0.004 660	11.42	0.992	6.82	0.85	1	NGC 1398
F03401−3003	0.005 040	11.11	0.803	7.87	0.76	1	NGC 1425
F03417−3600	0.004 630	10.46	0.514	−9.99	0.47	5	NGC 1436
F03451−3351	0.003 600	10.37	0.579	6.00	0.39	2	IC1993
F04305−5442	0.003 550	10.99	0.895	−9.99	0.63	5	NGC 1617
F05452−3415	0.003 070	10.50	0.713	7.22	0.69	1	NGC 2090
F06209−5942	0.007 560	10.89	0.516	7.40	0.53	161	ESO121−G026
F07184+8016	0.007 350	11.39	0.779	5.77	0.87	2	NGC 2336
F07525+6028	0.004 810	10.62	0.578	8.11	0.41	3	NGC 2460
F08547+0306	0.013 080	11.32	0.493	6.59	0.58	1	NGC 2713
F09076+0714	0.004 500	11.18	0.887	6.19	0.64	3	NGC 2775
F09134+7358	0.007 540	11.04	0.593	5.61	0.57	3	IC0529
F09186+5111	0.002 130	10.41	0.827	6.95	0.91	1	NGC 2841
F10068−2849	0.003 680	10.50	0.634	6.17	0.82	29	NGC 3137
F10312−2711	0.011 270	11.31	0.553	6.25	0.43	163	NGC 3285
F10346−2718	0.009 630	11.24	0.586	8.46	0.45	223	NGC 3312
F10456−2034	0.013 430	11.47	0.557	6.08	0.42	34	NGC 3450
F11089−3636	0.008 310	10.93	0.495	22.25	0.57	13	NGC 3573
F11163+1321	0.002 690	10.63	0.835	7.05	0.99	4	M065
F11549+5339	0.003 500	11.04	0.926	7.44	0.89	2	M109
F12015+3210	0.002 530	10.00	0.547	6.75	0.61	1	NGC 4062
F12133+1325	0.000 440	8.61	0.612	7.29	0.91	223	NGC 4216
F12149+3805A	0.000 810	9.05	0.567	10.44	1.22	1	NGC 4244
F12194−3531	0.009 790	11.12	0.519	6.99	0.51	6	ESO380−G019
F12234+1829	0.003 070	10.04	0.483	5.41	0.57	11	NGC 4394
F12257+2853	0.002 210	9.87	0.541	6.30	0.60	1	NGC 4448
F12259+1721	0.006 520	11.06	0.666	7.10	0.72	3	NGC 4450
F12329+1446	0.001 620	10.30	0.890	11.02	0.74	2	M091
F12374−1120	0.003 420	11.76	1.296	7.34	0.95	1	M104
F12407+0215	0.004 450	10.69	0.647	7.47	0.49	2	NGC 4643
F12415−4027	0.009 850	11.19	0.552	14.12	0.56	5	NGC 4650
F12474−1427	0.013 060	11.41	0.539	6.31	0.36	5	MCG-02-33-017
F13191−3622	0.001560	10.39	0.952	8.74	0.90	2	NGC 5102
F13331−3312	0.013 990	11.37	0.489	−9.99	0.38	3	NGC 5220
F13447−3041	0.014 900	11.55	0.552	5.71	0.27	5	NGC 5292
F13550−2904	0.008 920	11.32	0.660	6.56	0.80	2	IC4351
F14134+3627	0.009 590	11.12	0.528	6.96	0.79	2	NGC 5529
F14424+0209	0.005 750	11.36	0.870	7.45	0.89	2	NGC 5746
F15045+0144	0.008 530	10.99	0.514	6.26	0.64	2	NGC 5850
F15110−1405	0.006 640	11.03	0.643	6.09	0.59	1	NGC 5878
F17304+1626	0.010 400	11.24	0.553	25.21	0.49	1	NGC 6389
F17576−6625	0.014 480	11.56	0.569	−9.99	0.45	2	NGC 6389
F18300−5832	0.007 460	10.84	0.497	6.94	0.76	3	IC4721
F19049−6357	0.002 800	11.25	1.128	9.88	1.31	2	NGC 6744
F19101−6221	0.014 490	11.50	0.539	14.27	0.55	3	IC4831
F19139−6035	0.012 620	11.40	0.549	6.30	0.39	6	NGC 6769
F19227−5503	0.010 570	11.27	0.561	5.96	0.48	2	NGC 6788
F19588−5613	0.014 650	10.16	0.509	7.09	0.40	2	NGC 6848
F20134−5257	0.009 030	10.99	0.489	6.91	0.55	3	NGC 6887
F20210−4348	0.009 330	11.53	0.745	7.18	0.76	2	NGC 6902

Table 2. *– continued*

IRAS name	z	$L_{\rm opt}$	$\log_{10}\theta_{\rm pred}$	θ_{Planck}	$\log_{10}\theta_{\rm opt}$	ncirr	Name
Cool dust galaxies (cont.)							
F20346−5217	0.015150	11.48	0.510	13.36	0.30	2	NGC 6935
F20597−1700	0.004 920	10.57	0.543	17.33	0.63	1	IC5078
F21029−4822	0.017 200	11.63	0.529	14.32	0.43	3	ESO235−G057
F21142−6358	0.010 490	11.21	0.534	6.9	0.51	4	IC5096
F21596−1909	0.008 790	11.14	0.576	8.17	0.51	4	NGC 7183
F21598−2103	0.008 740	11.42	0.718	6.92	0.78	1	NGC 7184
F22061−4724	0.005 840	11.39	0.879	7.18	0.49	2	NGC 7213
F22369−6644	0.010 850	11.19	0.510	−9.99	0.59	1	NGC 7329
F22450−2234	0.011 140	11.56	0.683	−9.99	0.46	1	NGC 7377
F22521−3955	0.005 840	11.31	0.839	7.94	0.72	1	NGC 7410
F22543−4339	0.005 710	11.29	0.838	7.50	0.70	1	IC5267
F22544−4120	0.003 130	10.48	0.694	7.42	0.98	1	NGC 7424
F23105−2837	0.005 220	10.60	0.532	13.64	0.52	1	NGC 7513
F23120−4352	0.005 320	10.80	0.624	−9.99	0.66	1	NGC 7531
Cirrus galaxies							
F01319−2940	0.004 940	11.27	0.541	6.33	0.74	1	NGC 0613
F02207−2127	0.005 030	11.23	0.513	−9.99	0.78	1	NGC 0908
F02441−3029	0.004 240	11.41	0.678	6.32	0.98	4	NGC 1097
F03075−2045	0.005 350	11.44	0.592	5.92	0.87	1	NGC 1232
F03207−3723	0.005 870	12.01	0.836	11.92	1.05	4	NGC 1316
F03316−3618	0.005 460	11.57	0.648	7.37	1.05	2	NGC 1365
F03404−4722	0.003 590	11.03	0.560	6.9	0.81	2	NGC 1433
F04022−4329	0.002 990	10.87	0.559	6.8	0.95	1	NGC 1512
F04101−3300	0.003 470	11.04	0.580	9.2	1.10	1	NGC 1532
F04188−5503	0.005 020	11.34	0.569	5.58	0.92	8	NGC 1566
F04449−5920	0.004 440	11.18	0.543	6.88	0.92	117	NGC 1672
F05035−3802	0.004 040	11.13	0.559	5.51	0.72	2	NGC 1792
F07365−6924	0.004 890	11.27	0.546	5.3	0.81	7	NGC 2442
F08491+7824	0.004 670	11.22	0.541	7.71	0.69	4	NGC 2655
F08495+3336	0.001 370	10.36	0.643	6.87	0.98	1	NGC 2683
F09293+2143	0.001 830	10.77	0.723	7.78	1.10	4	NGC 2903
F10126+7338	0.009 350	11.86	0.559	5.24	0.59	1	NGC 3147
F10407+2511	0.001 930	10.55	0.589	6.95	0.85	1	NGC 3344
F10413+1157	0.002 590	10.88	0.627	7.41	0.88	3	M095
F10441+1205	0.002 990	11.08	0.664	6.31	0.88	3	M096
F11032+0014	0.002 670	11.20	0.773	5.9	1.04	7	NGC 3521
F11176+1315	0.002 430	11.06	0.744	6.64	0.97	2	M066
F11176+1351	0.002 810	11.04	0.671	7.13	1.17	4	NGC 3628
F12006+4448	0.002 340	10.56	0.511	6.03	0.72	1	NGC 4051 Seyf1
F12163+1441	0.008 030	11.70	0.545	7.08	0.75	222	M099
F12193+0445	0.005 220	11.43	0.597	5.25	0.81	7	M061
F12203+1605	0.005 240	11.49	0.626	7.87	0.88	33	M100
F12239+3130	0.002 390	10.63	0.537	−9.99	0.56	2	NGC 4414
F12294+1441	0.007 610	11.91	0.674	5.63	0.85	4	M088
F12334+2814	0.002 690	10.75	0.545	6.19	1.04	1	NGC 4559
F12410+1151	0.004 700	11.14	0.498	5.51	0.46	3	NGC 4647 (or 0.85 M60?)
F12464−0823	0.004 650	11.41	0.638	6.17	0.59	3	NGC 4699
F12498−0055	0.004 130	11.20	0.584	6.87	0.77	1	NGC 4753
F12542+2157	0.001 360	10.80	0.866	6.7	1.02	3	M064
F13086+3719	0.003 160	11.03	0.615	5.24	0.76	2	NGC 5005
F13170−2708	0.007 230	11.48	0.481	6.54	0.62	1	NGC 5078
F13277+4727	0.001 540	10.86	0.842	8.61	1.05	5	M051a
F13350+0908	0.003 840	10.93	0.481	6.43	0.79	1	NGC 5248
F22347+3409	0.002 720	11.07	0.700	6.97	1.06	53	NGC 7331
F23552−3252	0.000 770	9.83	0.629	6.85	0.98	1	NGC 7793

For each of these objects, we used an SDSS *i*-band optical image to trace the optical surface brightness profile from stellar emission after smoothing by a Gaussian matched to the size of the 250 μm SPIRE beam, and then compared this to the 250 μm surface brightness profile resulting from dust emission. The surface brightness profiles for this calculation were produced using the IRAF ellipse package and are plotted in Figs 6L and 7. In all cases, the optical and sub-mm surface brightness profiles are clearly different.

This is most obvious in NGC 5701, where there is a large ring of cold dust located outside most of the optical light distribution

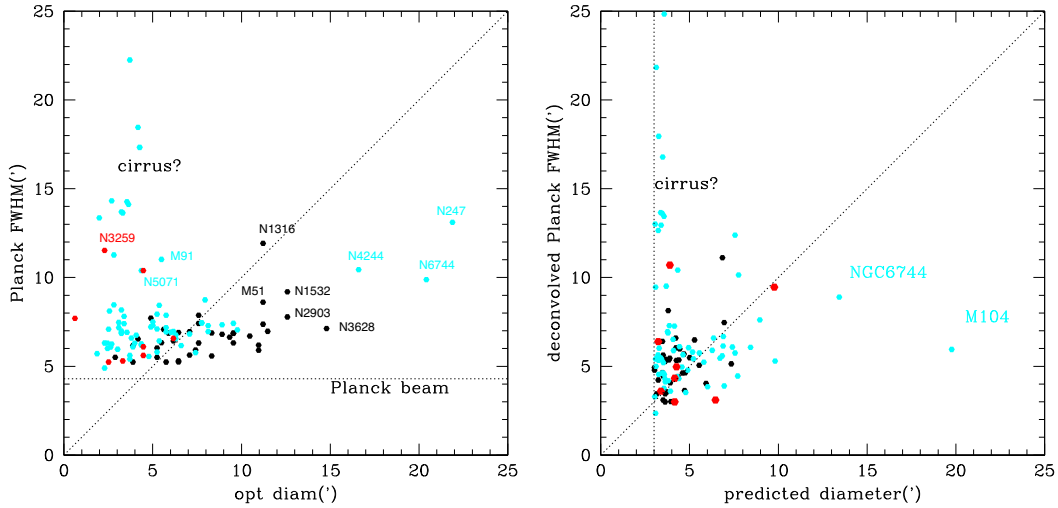

Figure 3. L: observed *Planck* 857 GHz FWHM versus optical diameter (arcmin) for standard cirrus galaxies ($\psi = 5$, black), cool cirrus galaxies ($\psi = 1$, cyan) and cold cirrus galaxies ($\psi = 0.1$, red). The dotted line denotes the *Planck* 857 GHz beam (FWHM). R: deconvolved *Planck* 857 GHz FWHM versus predicted sub-mm diameter (arcmin) for standard cirrus galaxies ($\psi = 5$, black), cool cirrus galaxies ($\psi = 1$, cyan) and cold cirrus galaxies ($\psi = 0.1$, red). Here the dotted line indicates the selection cutoff $\theta = 3.0$.

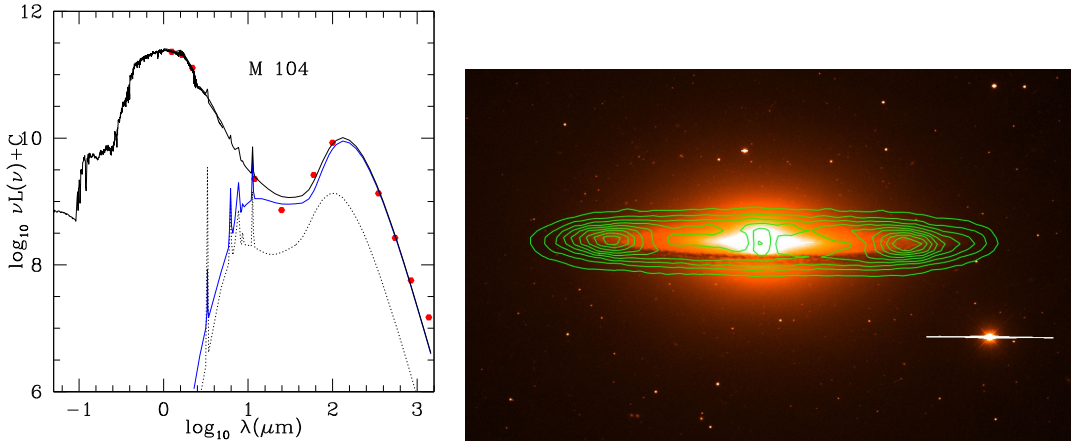

Figure 4. L: SED of M104, an outlier in Fig. 3R. R: 250 μm contour map of M104 superposed on *i*-band image. Much of the 250 μm emission arises from a ring of dust outside the main optical image.

(see Fig. 6R). This ring makes a substantial contribution to the integrated sub-mm emission, but the optical emission from starlight in this region is much less than in the more central regions of this object.

The dust emission in NGC 5669 (Fig. 8L) has a larger scalelength than the optical emission, with the ratio of sub-mm to optical surface brightness rising all the way to the edge of detectable emission in this object. Examination of the optical image suggests that this dust is associated with extended low surface brightness optical emission away from the galaxy's nucleus and bright spiral arms.

NGC 3049 (Fig. 8R) is an edge-on spiral, which makes this analysis a little less clear, and we see only a slight hint of changes to the optical to sub-mm surface brightness ratio in the outer parts of this object, or possibly weak sub-mm emission beyond the optically detected emission.

A further galaxy of interest, NGC 1617, classified as cool in Table 2, was observed as part of the HerMES survey (Oliver et al. 2012) since it lies in the Akari Deep Field South (ADF-S; Matsuura et al. 2011). Fig. 9L shows 250 μm contours superposed on an *r*-band image (from Hameed & Devereux 1999), while Fig. 9R shows 250 μm and *r*-band intensity profiles. In this case, a significant fraction of the sub-mm emission arises from two dust blobs that lie along the major axis to the north-west.

5 DISCUSSION AND CONCLUSIONS

The analysis of *Planck* 350 μm data shows very clearly that the galaxies whose SEDs require a cold dust component are indeed larger than normal galaxies and by an amount consistent with the interpretation that the surface brightness of the illuminating starlight is lower. The fact that this phenomenon of galaxies with cold dust did not show up in follow-up of *IRAS* galaxies reflects the fact that 60 μm selection biases samples towards galaxies with warmer dust. It needed the sub-mm sensitivity of *Herschel* and *Planck* to uncover this phenomenon.

The limited sub-mm mapping data available for these cold dust galaxies show that a variety of geometries may be involved. NGC 5701 shows a large ring of cold dust located outside most of the optical light distribution but in NGC 3049, the cold dust appears to be located closer to the centre of the galaxy.

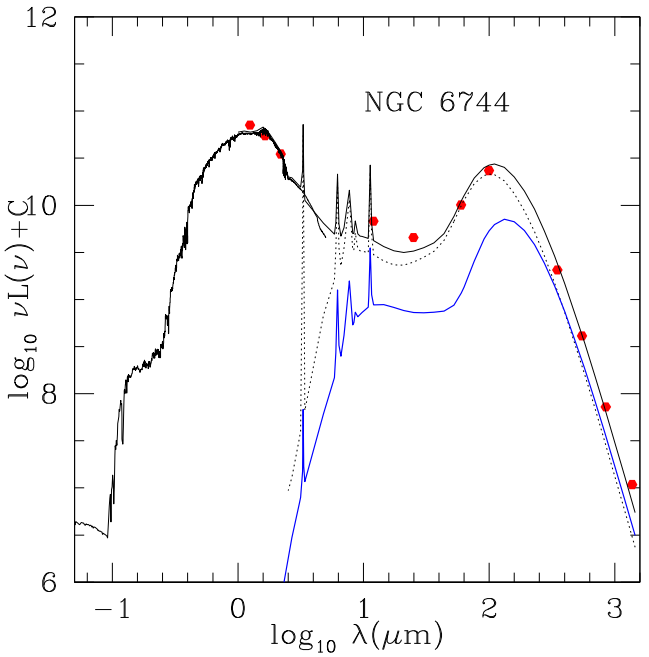

Figure 5. SED of NGC 6744, outlier in Fig. 3R.

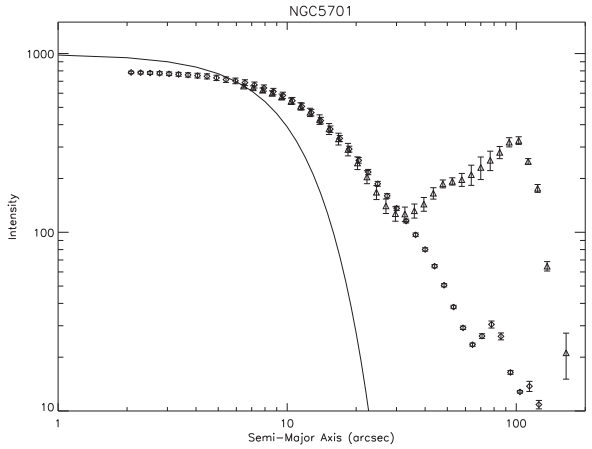

Figure 7. 250 μm and optical intensity profiles of NGC 5701. Diamonds indicate the *i*-band surface brightness derived from an SDSS image after it has been smoothed by a Gaussian matching the SPIRE beam at 250 μm, triangles show the 250 μm surface brightness from SPIRE observations. The solid line indicates a Gaussian model of the SPIRE 250 μm beam as given by the SPIRE Handbook http://herschel.esac.esa.int/Docs/SPIRE/spire_handbook.pdf. The true *Herschel* beam at 250 μm deviates somewhat from a pure Gaussian at radii beyond ∼20 arcsec at levels less than a few per cent (Griffin et al. 2013). This is insignificant to the current analysis. The surface brightness scale is arbitrary with the two profiles scaled to the same value at a semimajor axis radius of 10 arcsec. In this case, strong sub-mm emission arises in a ring of dust lying outside the main stellar distribution, which can be seen in Fig. 6R, leading to a region where the optical-to-submillimetre ratio is low.

It is unlucky that none of our cold dust galaxies is in the sample of nearby galaxies for which Bendo et al. (2015) have studied the 160/250 and 250/350 μm surface brightness profiles in detail. The next step will be to map some of these cold dust galaxies with ground-based sub-mm telescopes.

ACKNOWLEDGEMENTS

Herschel is an ESA space observatory with science instruments provided by European-led Principal Investigator consortia and with important participation from NASA. SPIRE has been developed by a consortium of institutes led by Cardiff University (UK) and including Univ. Lethbridge (Canada); NAOC (China); CEA, LAM (France); IFSI, Univ. Padua (Italy); IAC (Spain); Stockholm Observatory (Sweden); Imperial College London, RAL, UCL-MSSL, UKATC, Univ. Sussex (UK); and Caltech, JPL, NHSC, Univ. Colorado (USA). This development has been supported by national funding agencies: CSA (Canada); NAOC (China); CEA, CNES, CNRS (France); ASI (Italy); MCINN (Spain); SNSB (Sweden); STFC, UKSA (UK); and NASA (USA).

Based in part on observations obtained with *Planck* (http://www.esa.int/Planck), an ESA science mission with instruments and contributions directly funded by ESA Member States, NASA and Canada.

We thank George Bendo and an anonymous referee for helpful comments.

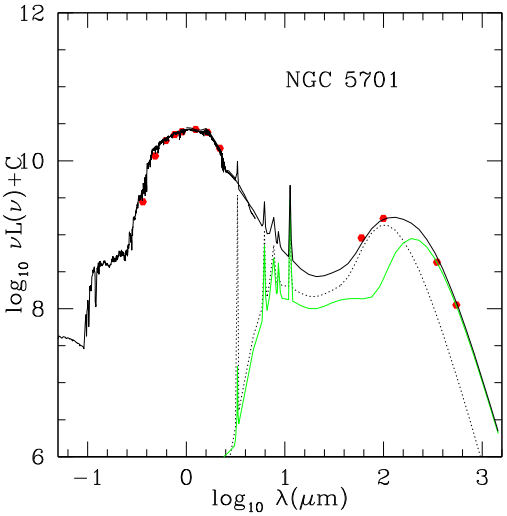

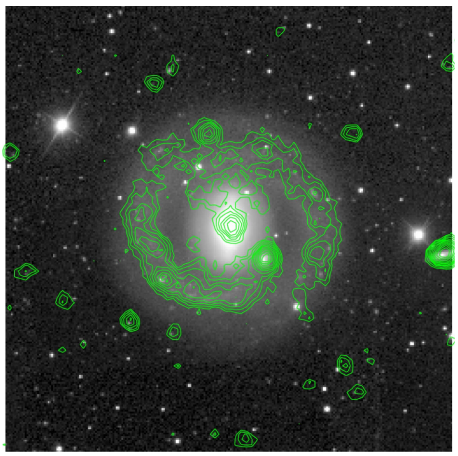

Figure 6. L: SED of NGC 5701. R: 250 μm map of NGC 5701. In this case the sub-mm emission arises from a ring of dust lying outside the main stellar distribution. The peak of emission to the SW of the nucleus is a chance superposition of a background $z = 0.04$ galaxy.

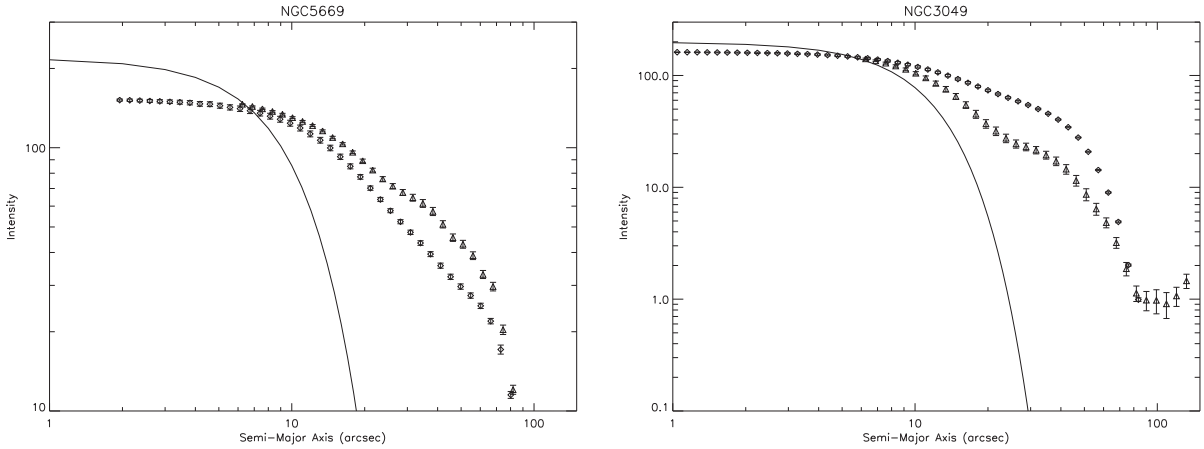

Figure 8. L: 250 μm and optical intensity profiles of NGC 5669. Symbols and scalings as in Fig. 6R. R: 250 μm and optical intensity profiles of NGC 3049. Symbols and scalings as in Fig. 6R.

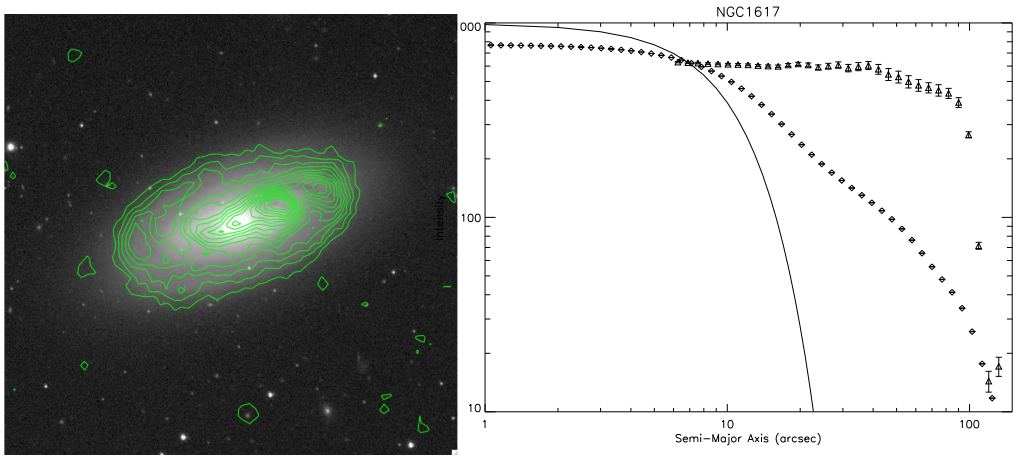

Figure 9. L: 250 μm contours of NGC 1617 superposed on *r*-band image. R: 250 μm and optical intensity profiles of NGC 1617. Symbols and scalings as in Fig. 6R.

REFERENCES

Bendo G. J. et al., 2006, ApJ, 645, 134
Bendo G. J. et al., 2015, MNRAS, 448, 135
Boselli A. et al., 2010, PASP, 122, 261
Bourne N. et al., 2013, MNRAS, 436, 479
Galametz M. et al., 2012, MNRAS, 425, 763
Griffin M. J. et al., 2010, A&A, 518, L3
Griffin M. J. et al., 2013, MNRAS, 434, 992
Hameed S., Devereux N., 1999, AJ, 118, 730
Ibar E. et al., 2013, MNRAS, 449, 2498
Kennicutt R. C. et al., 2010, PASP, 123, 1347
Matsuura S. et al., 2011, ApJ, 737, 2
Oliver S. J. et al., 2012, MNRAS, 424, 1614
Pilbratt G. et al., 2010, A&A, 518, L1
Planck Collaboration XVI, 2011, A&A, 536, A16
Rice W., Lonsdale C. J., Soifer B. T., Neugebauer G., Kopan E. L., Lloyd L. A., de Jong T., Habing H. J., 1988, ApJS, 68, 91
Rowan-Robinson M., 1992, MNRAS, 258, 787 (RR92)
Rowan-Robinson M. et al., 2005, AJ, 129, 1183
Rowan-Robinson M. et al., 2008, MNRAS, 386, 697
Rowan-Robinson M. et al., 2010, MNRAS, 409, 2
Rowan-Robinson M. et al., 2013, MNRAS, 428, 1958
Rowan-Robinson M. et al., 2014, MNRAS, 445, 3848
Smith D. J. B. et al., 2012, MNRAS, 427, 703
Symeonidis M. et al., 2013, MNRAS, 431, 2317
Wang L., Rowan-Robinson M., Norberg P., Heinis S., Han J., 2014, MNRAS, 442, 2739

This paper has been typeset from a TEX/LATEX file prepared by the author.